Planar Hall effect sensors with shape-induced effective single domain behavior

V. Mor,[1,a)] M. Schultz,[1] O. Sinwani,[1] A. Grosz,[2] E. Paperno,[2] and L. Klein[1]
[1]*Department of Physics, Nano-magnetism Research Center, Institute of Nanotechnology and Advanced Materials, Bar-Ilan University, Ramat-Gan 52900, Israel*
[2]*Department of Electrical and Computer Engineering, Ben-Gurion University of the Negev, P.O. Box 653, Beer-Sheva 84105, Israel*

(Presented 1 November 2011; received 23 September 2011; accepted 21 December 2011; published online 13 March 2012)

We show that shape anisotropy induces effective single domain behavior in elliptical structures of thin permalloy films with long axis ranging between several microns to several millimeters, provided that the ratio of the film long and short axes is large enough. We also show that the thin film elliptical structures exhibit a wide range of effective anisotropy fields, from less than 10 Oe up to more than 100 Oe. We discuss the advantage of shape anisotropy in the fabrication of planar Hall effect sensors with high field resolution. © *2012 American Institute of Physics*. [doi:10.1063/1.3680084]

The longitudinal and transverse resistivities of polycrystalline ferromagnetic films, for which the crystal symmetry effects are averaged out, depend on the angle θ between the electric current (**J**) and the magnetization (**M**) as follows:

$$\rho_{xx} = \rho_{\perp} + (\rho_{\parallel} - \rho_{\perp})\cos^2\theta, \tag{1}$$

$$\rho_{xy} = \frac{1}{2}(\rho_{\parallel} - \rho_{\perp})\sin 2\theta, \tag{2}$$

where $\rho_{\parallel}$ and $\rho_{\perp}$ are the resistivities parallel and perpendicular to the magnetization, respectively. Equation (1) describes the anisotropic magnetoresistance effect, whereas Eq. (2) describes the planar Hall effect (PHE).[1,2]

Magnetic sensors based on PHE usually use patterned magnetic films with effective single domain behavior. This is usually achieved by growth-induced magnetic anisotropy, either by growing the film in a magnetic field[3] or by exchange biasing the film with an antiferromagnetic layer.[4,5] These methods yield a single easy axis of magnetization that aligns the magnetization with the current when no field is applied. When a field perpendicular to the easy axis (in the film plane) is applied, the magnetization rotates uniformly and reversely. The change in ρ_{xy} due to this rotation is used to detect the magnitude of the component of the field which is perpendicular to the easy axis.

Here we show that shape anisotropy can be reliably used for achieving effective single domain behavior. Moreover, this method has unique advantages in the design of sensing devices based on the PHE. We also show that shape induced anisotropy can be approximated analytically and that single domain behavior can be induced in a very wide range of parameters provided the axes ratio of the ellipses is large enough.

To manufacture the sensors, we sputter permalloy films capped with tantalum on Si substrates in an UHV-evaporation and sputtering system (BESTEC). We pattern the elliptical sensors with an e-beam high resolution lithography system (CRESTEC) using either lift-off or Ar^+ milling. Leads and contact pads are deposited in a second stage. Figure 1 shows one of the sensors whose performance is reported here. Response measurements are performed using a Helmholtz coils system with a rotating sample stage having an angle resolution of 0.03^o. The sample is connected electrically to a switch box (Keithley 7001), a current source (Keithley 2400), and a nanovoltmeter (Keithley 2182). Sensitivity threshold (equivalent magnetic noise) measurements are performed at 1 Hz with the experimental setup shown in Fig. 2.

Figure 3 presents two types of experiments that demonstrate the effective single domain behavior of our elliptical sensors. The dimensions of the ellipse are 2 mm length, 0.25 mm width, and 60 nm thickness. Figure 3(a) shows the normalized PHE measured across the permalloy ellipse as a function of the angle α between **H** and ***J***. **J** is applied along the ellipse long axis. For each angle, the voltage is measured twice: with H = 100 Oe (the filled symbols) and H = 0 (the unfilled symbols). The voltage measured in the latter case indicates that for each α, **M** fully returns to the easy axis, and the variations in the zero-field signals are consistent with the expected effect of a small ambient field.

Figure 3(b) shows a sharp switching behavior of the measured PHE as a function of **H** at $\alpha = 130^o$ relative to the long axis of the ellipse. This type of behavior indicates effective single domain behavior with effective uniaxial anisotropy along the long axis of the ellipse, which is usually described by the Stoner–Wohlfarth Hamiltonian,

$$\mathcal{H} = K_u \sin^2\theta - M_s H\cos(\alpha - \theta), \tag{3}$$

where M_s is the saturation magnetization, K_u is the magnetic anisotropy constant, θ is the angle between M_s and the easy axis, and α is the angle between the external magnetic field **H** and the easy axis.

a)Author to whom correspondence should be addressed. Electronic mail: vladislav.mor@gmail.com.

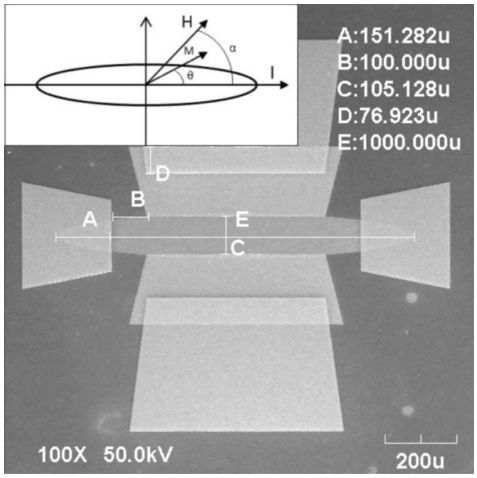

FIG. 1. Scanning electron microscope image of a typical PHE sensor. The elliptical part is made of permalloy capped with tantalum. Current is driven along the long axes through gold leads connected to the contact leads. Voltage is measured via the tantalum and gold leads connected to the contact pads. The inset shows the directions of the magnetic field (**H**) and the magnetization **M** relative to the current (**I**).

Figure 3(d) shows the dependence of the switching field (H_s) on α. The line is the expected for coherent rotation[6]

$$H_s(\alpha) = \frac{H_k}{\left[\sin^{2/3}\alpha + \cos^{2/3}\alpha\right]^{3/2}}, \tag{4}$$

where H_k is the anisotropy field defined as $2K_u/M_s$. We note that for α close to 180° the experimental points deviate from the theoretical prediction, indicating that in this narrow range of angles the magnetization reversal cannot be described in terms of coherent rotation. This, however, does not affect the functionality of our sensors, which are used to detect fields much smaller than the anisotropy field.

To determine the effective H_k of our sensors, we apply a small field perpendicular to the easy axis and measure the slope of θ versus $H_\perp$. Figure 4 represents the experimentally extracted H_k for elliptical sensors in a wide range of sizes as a function of c/b, where c is the film thickness, and b is the short axis of the ellipse.

We compare now the observed behavior with that of an ellipsoid of similar dimensions whose response can be studied analytically. For ellipsoids, one can define and calculate demagnetization factors, which have the following form in the limit $a \geq b \gg c$:[7]

$$\frac{N_a}{4\pi} = \frac{c}{a}(1-e^2)^{1/2}\frac{K-E}{e^2}, \tag{5}$$

$$\frac{N_b}{4\pi} = \frac{c}{a}\frac{E-(1-e^2)K}{e^2(1-e^2)^{1/2}}, \tag{6}$$

$$\frac{N_c}{4\pi} = 1 - \frac{E}{a(1-e^2)^{1/2}}, \tag{7}$$

where a, b, and c are the axes of the ellipsoid. N_a, N_b, and N_c are the demagnetizing factors (corresponding to a, b, and c respectively). K is a complete elliptic integral of the first kind and E is a complete elliptic integral of the second kind,

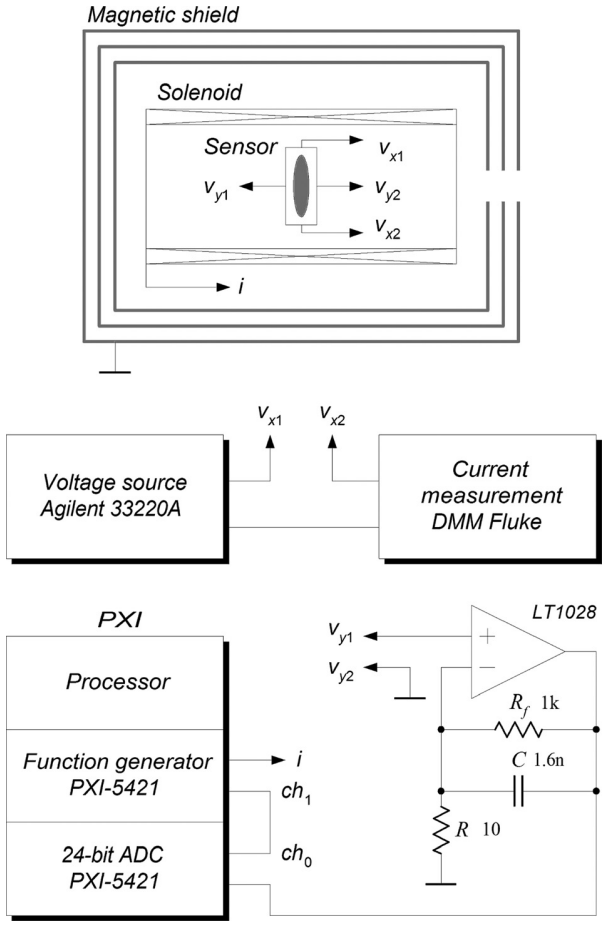

FIG. 2. Experimental setup for measuring the sensor resolution. The setup includes a three-shell magnetic shield, a voltage source, a current measurement instrument (to apply a bias), a preamplifier, and a National Instruments personal computer-based platform for test, measurement, and control (PXI).

whose argument is $e = (1 - b^2/a^2)^{1/2}$. The behavior of the sensors when **H** is applied in the *ab* plane can be described by the Stoner–Wohlfarth Hamiltonian where the anisotropy constant K_u is given by $K_u = (1/2)M_s^2(N_b - N_a)$.

In the limit $a \gg b \gg c$ we use the asymptotic expansions of K and E (Ref. 8) to obtain

$$H_k \sim 4\pi M_s \frac{c}{b} \sim 10,807\frac{c}{b}Oe. \tag{8}$$

We compare the analytical approximation with the experimental results (see Fig. 4) and note that the experimental value of H_k has a lower bound. This is due to the effect of the intrinsic anisotropy of the permalloy film, which is growth dependent and usually varies between 5 and 10 Oe. We compare the analytical approximation with OOMMF (Ref. 9) simulations and note that the approximation in Eq. (8) is quite good for $a/b \geq 8$.

We have also performed simulations for ellipses and rectangles and have found that the analytical approximation is better for elongated ellipses.

The simulations also indicate the effective single domain behavior for ellipsoids and ellipses in a very wide range of sizes, whereas rectangular samples are much less stable. The ellipses with axes ratio of 6 : 1 and above behave quite

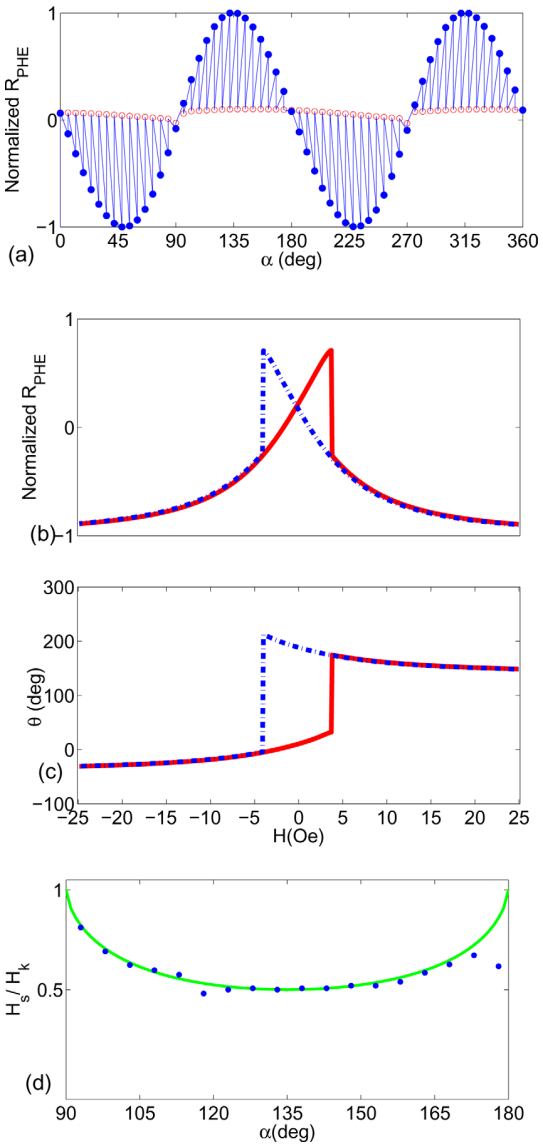

FIG. 3. (Color online) Effective single-domain behavior of large elliptical sensors. (a) Normalized PHE measured across an elliptical sensor as a function of the angle α between **H** and **J**. The dimensions of the ellipse are 2 mm length, 0.25 mm width, and 60 nm thickness, and **J** is applied along its long axis. For each α, the voltage is measured twice: with H = 100 Oe (filled symbols) and with H = 0 (unfilled symbols). (b)The PHE as a function of **H** at an angle $\alpha = 130^{o}$ for elliptical sensor with dimensions 1 mm length, 0.125 mm width, and 60 nm thickness. (c) The corresponding θ for the measurements shown in b. (d) The switching field divided by H_k as a function of α. The line is a fit to the Stoner–Wohlfart model.

like a single domain particle and the behavior improves with increasing axes ratio.

Surprisingly, the single-domain-like behavior is observed even for very large ellipses. This has a practical importance since the big ellipses have a very small H_k, which means that their sensitivity $S = (V_{\mathrm{PHE}}/I)(1/H_{\perp}) \propto 1/H_k$ is higher. Here, V_{PHE} is the measured transverse voltage, I is the current through the sensor, $H_{\perp}$ is the field applied perpendicular to the easy axis. We have obtained H_k as small as 8 Oe and S as big as 200 Ω/T.

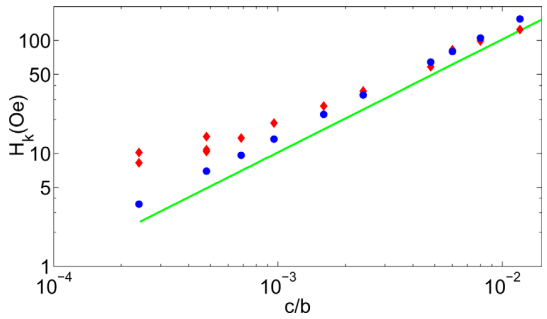

FIG. 4. (Color online) The experimental (diamonds) and simulated (dots) shape anisotropy field for ellipses as a function of the axes ratio b/c. The line represents the theoretical anisotropy field of ellipsoids [Eq. (8)].

The field resolution of our sensors is determined using the setup described in Fig. 2. First, we measure the sensitivity of sensor. Second, we measure the amplitude spectral density of the noise, and then translate the noise spectral density into the sensitivity threshold by dividing it by the sensitivity.

To measure the sensitivity, we apply an external magnetic field by a long solenoid connected to a function generator, bias the sensor with a voltage source, amplify the sensor output by an ultra-low noise preamplifier, and sample the preamplifier output by a 24 bit analog to digital convertor. The amplifier noise is negligible compared to the 1/f noise of the sensor at a given ac bias current, and there is no need to use either Wheatstone Bridge or cross-correlation techniques. All the measurements are performed in a three-layer magnetic shield. Using this setup, we find that our best sensors have at 1 Hz field resolution of about 0.6 $nT/\sqrt{Hz}$.

We believe that H_k can be further reduced by more than an order of magnitude, which would increase S accordingly. In addition, a flux concentrator can be used to amplify the measured field.[10,11] Therefore, it appears likely that further improvement of the field resolution by orders of magnitude is within reach.

Such sensors could be very useful for applications not only for their high resolution but also because they offer the possibility of fabricating on a single device, multiple sensors with a wide range of H_k along different directions—features that open new opportunities for PHE sensors.

L.K. acknowledges support by the Israel Science Foundation founded by the Israel Academy of Science and Humanities. The content of this manuscript is patent pending.

[1]C. Goldberg and R. E. Davis, Phys. Rev. **94**, 1121 (1954).
[2]F. G. West, J. Appl. Phys. **34**, 1171 (1963).
[3]A. Schuhl, F. N. Van Dau, and J. R. Childress, Appl. Phys. Lett. **66**, 2751 (1995).
[4]C. D. Damsgaard *et al.*, Sens. Actuators, A **56**, 103 (2009).
[5]A. Nemoto, Appl. Phys. Lett.**74**, 4026 (1999).
[6]C. Tannous and J. Gieraltowski, Eur. J. Phys. **29**, 475 (2008).
[7]J. A. Osborn, Phys. Rev. **67**, 351 (1945).
[8]A. Gasull *et al.*, Pac. J. Math. **202**, 341 (2002).
[9]The publicly available object oriented micromagnetic framework, http://math.nist.gov/oommf.
[10]F. Montaigne *et al.*, Sens. nd Actuators, A **81**, 324 (2000).
[11]F. N. Van Dau *et al.*, The 8th International Conference on Solid-State Sensors and Actuators, and Eurosensors IX, Transducers '95, Stockholm, Sweden, June 25–29, 1995, p. 292.